Engineering Applications of Computational Fluid Mechanics Vol. 4, No. 2, pp. 196–208 (2010)

DETAILED INUNDATION MODELLING USING HIGH RESOLUTION DEMs

Sébastien Erpicum*[†], Benjamin Dewals*[#], Pierre Archambeau*,
Sylvain Detrembleur* and Michel Pirotton*

** Research unit of Hydrology, Applied Hydrodynamics and Hydraulic Constructions (HACH), ArGEnCo Department – MS²F – University of Liege (ULg), Chemin des Chevreuils, 1 B52/3 B-4000 Liege, Belgium*
[†] E-Mail: S.Erpicum@ulg.ac.be (*Corresponding Author*)
[#] Belgian National Fund for Scientific Research FRS – FNRS

ABSTRACT: With the availability of high resolution DEMs, relevant and detailed inundation maps may now be routinely computed provided that suitable flow models are available. The full 2D flow model presented in this paper has been used to compute such maps on 800 km of the main rivers of the Walloon Region in Belgium. The use of grid spacing of 1 m, similar to the DEM resolution, enables the accurate prediction of the pattern of flood depth. This is confirmed by several application examples, which also demonstrate the ability of the model to reproduce depth measurements for a wide range of flood discharges without the need for recalibration of the roughness coefficient. The numerical model has been systematically validated by comparison with observations during recent real flood events. It shows a very good agreement with field data, in particular the free surface elevations and inundation extension.

Keywords: SWE, finite volume, high resolution DEM, inundation mapping

1. INTRODUCTION

In the global framework of recurrent large flood events all over the world and in Europe in particular, relevant and detailed inundation maps represent a tool of prime interest to help decision makers in defining land use and housing policies, to inform people living in flood-prone areas, to improve emergency planning and to help insurance companies to assess the risks associated with flooding (Bradbrook, Waller and Morris, 2005; Merz, Blöschl and Humer, 2008). To be usable in practise, such maps should however be drawn in a scientific and objective manner, using high accuracy topographic data. They should also cover a large range of probabilistic flood events, taking into account possible climate evolution, and not only represent well documented extreme events from the past. Finally, they have to be easy to update regarding significant changes in the river bed topography or floodplain characteristics.
In this scope, hydraulic numerical modelling can provide relevant and reliable results, especially when the solvers are able to use the accurate and very dense topographic information provided today by high resolution Digital Elevation Models (DEMs) derived from airborne LIDAR or on boat sonar (McMillan and Brasington, 2007).
A significant evolution in the flood inundation numerical models using such DEMs has been observed over the last decades. Bates and De Roo (2000) clearly summarized this evolution, ranging from planar water surface model without channel or floodplain routing (Priestnall, Jaafar and Duncan, 2000) to simplified 2D solvers (e.g. Bradbrook, Waller and Morris, 2005) or coupled approaches applying different more or less sophisticated models in the channel and the floodplain (e.g. Bates and De Roo, 2000; McMillan and Brasington, 2007) and up to 2D models providing a full solution of the Saint-Venant equations on the whole inundated area (e.g. Mignot, Paquier and Haider, 2006; Erpicum et al., 2007).
The application of fully 2D models on the whole inundated area provides reliable distributed results, such as water depths and velocity fields, even in dense urban areas (Mignot, Paquier and Haider, 2006). These results are of prime interest to estimate the damage caused by the floods (Dutta, Herath and Musiake, 2003), and thus the risk associated with flooding. Once the parameters of the model have been calibrated, and especially roughness coefficient, inundation modelling can be performed for a set of pertinent probabilistic extreme events in order to fully characterise the so-called "inundation hazard" along a river.
McMillan and Brasington (2007) point out that the main drawback of actual flow solvers lies in

Received: 24 Aug. 2009; Revised: 19 Oct. 2009; Accepted: 3 Nov. 2009

their inability to make optimal use of the very dense topography information provided today by airborne LIDAR for example. In this paper, a fully 2D hydraulic numerical model is presented, which has been used to compute flood inundation maps on 800 km of the main rivers in the Walloon Region in Belgium with a spatial resolution as fine as 1 m. Coupled with a suitable treatment of high resolution DEMs to supply accurate topographical information for hydrodynamic simulations, the solver allows computing inundation maps at the scale of the streets and buildings in urban areas. The simplicity and the efficiency of the finite volume numerical scheme enable indeed the model to solve the classical shallow water equations (SWE) on computation grids with as many as one million meshes (3 millions unknowns) using standard computers (3.4 Ghz – 4 Gb RAM) with a computation time in the order of a couple of days.

Following the detailed description of the solver features, several validation examples and applications for flood inundation mapping are presented in detail.

2. FLOW MODEL

2.1 Mathematical model

The flow model is based on the two-dimensional depth-averaged equations of volume and momentum conservation. In the "shallow-water" approach, it is basically assumed that velocities normal to the main flow plane are significantly smaller than those in this main flow direction. Consequently, the pressure field is almost hydrostatic everywhere.

The large majority of flows occurring in rivers, even highly transient, can reasonably be seen as shallow everywhere, except in the vicinity of some singularities (e.g. weirs). Indeed, vertical velocity components remain generally low compared to velocity components in the horizontal plane and, consequently, flows may be considered as mainly two-dimensional. Thus, the approach presented in this paper is suitable for many of the problems encountered in river management, and especially flood inundation mapping.

The conservative form of the depth-averaged equations of volume and momentum conservation can be written as follows, using vector notations:

$$\frac{\partial \mathbf{s}}{\partial t}+\frac{\partial \mathbf{f}}{\partial x}+\frac{\partial \mathbf{g}}{\partial y}+\frac{\partial \mathbf{f}_{\mathrm{d}}}{\partial x}+\frac{\partial \mathbf{g}_{\mathrm{d}}}{\partial y}=\mathbf{S}_0-\mathbf{S}_{\mathrm{f}} \tag{1}$$

where $\mathbf{s}=\left[h \quad hu \quad hv\right]^{\mathrm{T}}$ is the vector of the conservative unknowns. $\mathbf{f}$ and $\mathbf{g}$ represent the advective and pressure fluxes in directions x and y, while $\mathbf{f}_{\mathrm{d}}$ and $\mathbf{g}_{\mathrm{d}}$ are the diffusive fluxes:

$$\mathbf{f}=\begin{pmatrix} hu \\ hu^2+\frac{1}{2}gh^2 \\ huv \end{pmatrix},\ \mathbf{g}=\begin{pmatrix} hv \\ huv \\ hv^2+\frac{1}{2}gh^2 \end{pmatrix} \tag{2}$$

$$\mathbf{f}_{\mathrm{d}}=-\frac{h}{\rho}\begin{pmatrix} 0 \\ \sigma_x \\ \tau_{xy} \end{pmatrix},\ \mathbf{g}_{\mathrm{d}}=-\frac{h}{\rho}\begin{pmatrix} 0 \\ \tau_{xy} \\ \sigma_y \end{pmatrix} \tag{3}$$

$\mathbf{S}_0$ and $\mathbf{S}_f$ designate respectively the bottom slope and the friction terms:

$$\mathbf{S}_0=-gh\left[0 \quad \partial z_b/\partial x \quad \partial z_b/\partial y\right]^{\mathrm{T}} \tag{4}$$

$$\mathbf{S}_{\mathrm{f}}=\left[0 \quad \tau_{\mathrm{bx}}\Delta\Sigma/\rho \quad \tau_{\mathrm{by}}\Delta\Sigma/\rho\right]^{\mathrm{T}} \tag{5}$$

In Eqs. (1) to (5), t is the time, x and y the space coordinates, h the water depth, u and v the depth-averaged velocity components, z_b the bottom elevation, g the gravity acceleration, ρ the density of water, τ_{bx} and τ_{by} the bottom shear stresses, σ_x and σ_y the turbulent normal stresses, and τ_{xy} the turbulent shear stress. Consistently with Hervouet (2003),

$$\Delta\Sigma=\sqrt{1+\left(\partial z_{\mathrm{b}}/\partial x\right)^2+\left(\partial z_{\mathrm{b}}/\partial y\right)^2} \tag{6}$$

reproduces the increased friction area on an irregular (natural) topography (Dewals, 2006).

2.2 Friction modelling

The bottom friction is conventionally modelled with empirical laws, such as the Manning formula. The model enables the definition of a spatially distributed roughness coefficient to represent different land-uses, floodplain vegetations or sub-grid bed forms. In addition, the friction along side walls is reproduced through a process-oriented formulation developed by Dewals (2006). Finally, friction terms become:

$$\frac{\tau_{\mathrm{bx}}}{\rho}=gh\,u\left[\sqrt{u^2+v^2}\,\frac{n_{\mathrm{b}}^2}{h^{4/3}}+u\sum_{k_x=1}^{N_x}\frac{4}{3}\frac{n_{\mathrm{w}}^2}{h^{1/3}\Delta y}\right] \tag{7}$$

$$\text{and}\quad \frac{\tau_{\mathrm{by}}}{\rho}=gh\,v\left[\sqrt{u^2+v^2}\,\frac{n_{\mathrm{b}}^2}{h^{4/3}}+v\sum_{k_y=1}^{N_y}\frac{4}{3}\frac{n_{\mathrm{w}}^2}{h^{1/3}\Delta x}\right] \tag{8}$$

where the Manning coefficients n_b and n_w characterize respectively the bottom and the side-walls roughness. These relations have been written for Cartesian grids, such as used in the present study.

The internal friction might be reproduced by applying a proper turbulence model. For SWE, various approaches are proposed in the literature, from rather simple algebraic expressions of turbulent viscosity (Fischer et al., 1979; Hervouet, 2003) to more complex mathematical models with 1 or 2 additional equations (Rastogi and Rodi, 1978; Rodi, 1984; Erpicum, 2006). Nevertheless, for the computations presented in this paper, no turbulence model has been used. All friction effects are thus globalized in the bottom and wall friction terms in a value of the roughness coefficient calibrated based on real events data.

2.3 Grid and numerical scheme

The solver includes a mesh generator and deals with multiblock grids (Erpicum, 2006). Within each block, the grid is Cartesian to take advantage of the lower computation time and the gain in accuracy provided by this type of structured grids compared to unstructured ones.

The multiblock features increase the domain area which can be discretized with a constant cells number and enable local mesh refinements close to areas of interest. It is thus a solution to overcome the main drawback of Cartesian grid, i.e. the high number of cells needed for a fine enough discretization of complex geometries. Moreover, it allows combining local high precision with strong computation speed requirements.

In addition, an automatic grid adaptation technique restricts the simulation domain to the wet cells to decrease the number of computational elements. Wetting and drying of cells is handled free of volume and momentum conservation error by means of an iterative resolution of the continuity equation (Erpicum, 2006). A four-step procedure is followed at each temporal step of integration:

1. Continuity equation is evaluated,
2. Algorithm detects the cells with a negative flow depth to reduce the outflow unit discharges such that the computed water depth in these cells is strictly equal to zero,
3. Since these flux corrections may induce the drying in cascade of neighbouring cells, steps 1 to 3 are repeated iteratively, and
4. Momentum equations are finally computed based on the corrected unit discharge values.

In most practical applications, no more than two iterations are necessary, thus keeping the computation cost limited.

Eq. (1) is discretized in space with a finite volume scheme. This ensures a correct mass and momentum conservation, which is a must for handling properly discontinuous solutions such as moving hydraulic jumps. As a consequence, no assumption is required regarding the smoothness of the solution. Reconstruction at cell interfaces can be performed with a constant or linear approach. For the latter, together with slope limiting, a second-order spatial accuracy is obtained.

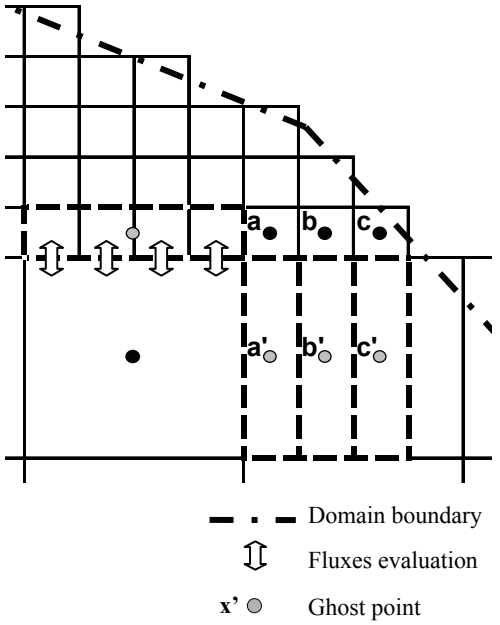

Fig. 1 Border between two adjacent blocks on a Cartesian multiblock grid – Ghost points for the reconstruction of the variables.

In a similar way, variables at the border between adjacent blocks are reconstructed linearly, using in addition ghost points as depicted in Fig. 1. The value of the variables at the ghost points is evaluated from the value of the adjacent cells. Moreover, to ensure conservation properties at the border between adjacent blocks and thus to compute accurate volume and momentum balances, fluxes related to the larger cells are computed at the level of the finer ones.

Appropriate flux computation has always been a challenging issue in computational fluid dynamics. The fluxes **f** and **g** are computed by a Flux Vector Splitting (FVS) method, where the

upwinding direction of each term of the fluxes is simply dictated by the sign of the flow velocity reconstructed at the cell interfaces. It can be formally expressed as:

$$\mathbf{f}^{+}=\begin{pmatrix} hu \\ hu^2 \\ huv \end{pmatrix} \quad ; \quad \mathbf{f}^{-}=\begin{pmatrix} 0 \\ gh^2/2 \\ 0 \end{pmatrix} \tag{9}$$

$$\mathbf{g}^{+}=\begin{pmatrix} hv \\ huv \\ hv^2 \end{pmatrix} \quad ; \quad \mathbf{g}^{-}=\begin{pmatrix} 0 \\ 0 \\ gh^2/2 \end{pmatrix} \tag{10}$$

where the superscripts + and − refer to, respectively, an upstream and a downstream evaluation of the corresponding terms. A Von Neumann stability analysis has shown that this FVS ensures a stable spatial discretization of the terms $\partial\mathbf{f}/\partial x$ and $\partial\mathbf{g}/\partial y$ in Eq. (1) (Dewals, 2006). Due to their diffusive character, the fluxes $\mathbf{f}_d$ and $\mathbf{g}_d$ can be determined by means of a centred scheme.

Besides low computation costs, this FVS has the advantages of being completely Froude independent and of facilitating the adequacy of discretization of the bottom slope term (Dewals et al., 2006 and 2008a).

2.4 Topography gradients

The discretization of the topography gradients is always a challenging task when setting up a numerical flow solver based on the SWE. The bed slope appears as a source term in the momentum equations. As a driving force of the flow, it has however to be discretized carefully, in particular regarding the treatment of the advective terms leading to the water movement, such as pressure and momentum.

The first step to assess topography gradients discretization is to analyse the situation of still water on an irregular bottom. In this case, the momentum equations are simplified and there are only two remaining terms: the advective term of hydrostatic pressure variation and the topography gradient. For example, regarding x-axis equation

$$\frac{g}{2}\frac{\partial h^2}{\partial x}=-gh\frac{\partial z_b}{\partial x} \tag{11}$$

The hydrostatic pressure gradient has to be exactly counterbalanced by the bottom slope term. Analytically, the equation can be written as

$$gh\frac{\partial Z}{\partial x}=0 \tag{12}$$

with Z the free surface elevation. In case of water at rest, the free surface gradient is equal to zero and thus the free surface is horizontal.

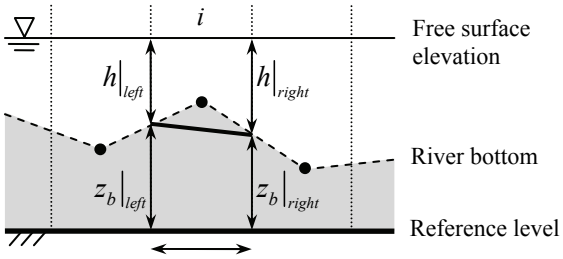

Fig. 2 Correspondence between the gradients of bottom elevation and water depth for water at rest.

In this case, assuming the bottom elevation and the water height are reconstructed coherently at the finite volume sides and their gradients are identically evaluated (Fig. 2). The left hand side of Eq. (11) can be written as

$$\frac{g}{2}\frac{\partial h^2}{\partial x}=gh\frac{\partial h}{\partial x} \tag{13}$$

The space discretization has to provide equivalent conservative and non conservative forms of the pressure gradient. According to the FVS characteristics, a suitable treatment of the topography gradient source term of Eq. (4) is thus a downstream discretization of the bottom slope and a mean evaluation of the corresponding water depths (Erpicum, 2006). For a mesh i and considering a constant reconstruction of the variables, the bottom slope discretization writes:

$$-gh\left.\frac{\partial z_b}{\partial x}\right|_i \rightarrow -g\frac{\left(h|_{i+1}+h|_i\right)}{2}\frac{\partial\left(z_b|_{i+1}-z_b|_i\right)}{\partial x} \tag{14}$$

where subscript $i+1$ refers to the downstream mesh along the x-axis.

This approach fulfils the numerical compatibility conditions defined by Nujic (1995) regarding the stability of water at rest. The final formulation is the same as the one proposed by Soares (2000) or Audusse (2004).

The formulation is suited to be used in both 1- and 2-D models, along x- and y- axis. Its very simple expression benefits directly from the simplicity of the original spatial discretization scheme.

Nevertheless, the formulation of Eq. (14) constitutes only a first step towards an adequate form of the topography gradient as it is not entirely suited regarding water in movement over an irregular bed. The effect of kinetic terms is not

taken into account and, consequently, poor evaluation of the flow energy evolution may occur when modeling flow, even stationary, over strongly irregular topography (Erpicum, 2006). No solution to this problem preserving the model potentiality to compute flow discontinuities (hydraulic jumps) has been found. Eq. (14) is thus used and the possible influence on flow energy evolution is accounted for in the roughness calibration procedure.

2.5 Time discretization

Since the model is applied to compute steady-state solutions, the time integration is performed by means of a 3-step first order accurate Runge-Kutta algorithm. A semi-implicit treatment of the bottom friction term is used, without requiring additional computational costs.
Writing Eq. (1) as

$$\frac{\partial \mathbf{s}}{\partial t} = \mathrm{R}(\mathbf{s}) - \mathbf{S}_f^* \mathbf{s} \tag{15}$$

with $\mathrm{R}(\mathbf{s})$ the vector of advective, pressure and diffusive fluxes and bottom slope term and $\mathbf{S}_f^*$ a diagonal matrix with the bottom friction term, equations for the time integration scheme over a time step Δt are

$$\mathbf{s}^{t+\Delta t} = \sum_{k=0}^{2} a_k \mathbf{s}^{(k)} \tag{16}$$

with $\mathbf{s}^{(0)} = \mathbf{s}^t$ and

$$\mathbf{s}^{(k)} = \frac{\mathbf{s}^t + \Delta t \mathbf{R}\left[\mathbf{s}^{(k-1)}\right]}{1 + \Delta t \mathbf{S}_f^{*(k-1)}} \quad \text{with } k = 1,2 \tag{17}$$

Values of the Runge-Kutta algorithm coefficients a_k equal to $a_0 = 0.15$, $a_1 = 0.4$ and $a_2 = 0.45$ provide adequate dissipation in time for steady state computation. Slight changes in the values of coefficients allow modifying the scheme dissipation properties and make it suitable for accurate transient computations (Lambert, 1973).
For stability reasons, the time step is constrained by the Courant-Friedrichs-Levy condition based on gravity waves:

$$\Delta t \le \frac{\Delta x}{c} \quad \text{with } c = |u| + \sqrt{gh} \text{ the wave celerity.} \tag{18}$$

2.6 Boundary conditions

For each application, the value of the specific discharge can be prescribed as an inflow boundary condition. The transverse specific discharge is usually set to zero at the inflow even if a different value can be used if necessary. In case of supercritical flow, a water elevation can be provided as additional inflow boundary condition.
The outflow boundary condition may be a water surface elevation, a Froude number or no specific condition if the outflow is supercritical. At solid walls, the component of the specific discharge normal to the wall is set to zero.

2.7 Automatic mesh refinement

An automatic mesh refinement technique is available to enhance the convergence rate towards accurate steady-state solutions (Archambeau, 2006). The computations are performed on several successive grids, starting from a very coarse one, gradually refined up to the finest one. When the hydrodynamic fields are almost stabilized, the solver automatically jumps onto the next grid. The successive "initial solutions" are interpolated from the coarser towards the finer grid in terms of both water elevations and discharges. This fully automatic method considerably reduces the number of cells and increases the time step in the first grids for a faster propagation of discharges and the filling of initially dry areas. Hence, it substantially decreases computation time, despite some extra computation time needed for meshing and interpolation operations (Dewals et al., 2008b).

2.8 Other features

The herein described model constitutes a part of the modelling system "WOLF", developed at the University of Liege. WOLF includes a set of complementary and interconnected modules for simulating free surface flows: process-oriented hydrology, 1D & 2D hydrodynamics, sediment or pollutant transport, air entrainment, the whole optionally coupled to an optimisation tool based on Genetic Algorithms (Archambeau, 2006; Dewals, 2006; Erpicum, 2006).
A user-friendly GIS interface (Archambeau, 2006), makes the pre- and post-processing operations very convenient. Import and export operations are easily implemented from and to various classical GIS tools. Different layers of maps can be handled to analyse information related to the topography, the ground characteristics, the vegetation density and the hydrodynamic fields.

3. TOPOGRAPHY DATA

Topography data quality is of prime importance regarding flood extension modelling. Indeed, errors of estimation of flood depths are generally lower than errors in elevation estimation of typical standard existing DEM (Bradbrook, Waller and Morris, 2005). Thus, the choice of DEM is likely to have a large impact on the final flood outlines.

For about a decade, high resolution, high accuracy topographic datasets have become increasingly available for inundation modelling in a number of countries. In Belgium, a data collection programme using airborne laser altimetry (LIDAR) has generated high quality topographic data covering the floodplains of most rivers in the southern part of the country. Simultaneously, the bathymetry of the main channel on navigable rivers has been surveyed by means of an echo-sonar technique.

Consequently, the poor and inaccurate topography information used for many years, i.e. 30 m of horizontal resolution with a precision of several meters in altitude, has been replaced by an exceptionally accurate data set since the laser and sonar precision in altitude can be 15 cm and the information density is one point per square meter. Such LIDAR based DEMs represent the best source of terrain data for flood modelling today (Sanders, 2007).

Regarding smaller non navigable rivers, cross sections information can be efficiently interpolated to generate the main channel bathymetry and to complete the floodplain laser data. However, in this case, special care has to be paid to possible singularities in the river bed and the DEM resulting from the interpolation procedure has often to be completed to represent the whole of the river channel details. This last procedure can be even more important and time consuming when the cross sections information dates from tens of years, as it is generally the case in several European countries.

The huge improvement in the quality of the main data set makes it possible to focus on proper physical values of the roughness coefficient rather than using it to assess the effect of blockage by buildings or of large irregularities of the topography. It allows also refining the flood extension forecasting at the scale of each house and street individually.

Since inundation flows may be extremely sensitive to some local topographic characteristics, such as for instance the exact height of a protection wall, a crucial step consists in validating and enhancing the DEM by removing residual obstacles not relevant to the flow (e.g. vegetation, trailers), by integrating additional sources of topographic data (including field survey) as well as the detailed geometry of flood protections and other hydraulic structures (weirs, water intake, etc). The large amount of data collected from those various sources is stored into an efficient database structure.

This last point also underlines the importance of the accuracy and especially the updating of the data to provide reliable numerical results. It is very useful to have a suitable storage of all the data sets to be able to quickly pick them up to update the maps to take into account modifications in the DEM.

4. METHODOLOGY FOR SYSTEMATIC INUNDATION MAPPING

Following a Regional Government decision in 2003, the solver WOLF2D, presented in this paper, has been chosen to be used to compute the official inundation hazard maps on 800 km of the main rivers of the Walloon Region in Belgium. This work has been performed in the scope of flood risk management, insurance of this risk, critical areas identification and climate change effects mitigation policy.

A 4-step modelling procedure has been elaborated and applied systematically for each river reach:

1. Elaboration from laser altimetry and sonar data (or cross sections) of the complete DEM (main riverbed and floodplains) with a grid resolution of 1 m by 1 m,
2. Validation and enhancement of the DEM by a field survey and the integration of additional geometric characteristics,
3. Flow modelling of past flood events with the purpose of calibrating and validating the roughness parameters,
4. Computation of the inundation maps for constant statistical flood discharge values with a 25-, 50- and 100-year return period.

Depending on the river width, steps 2 to 4 are conducted with a grid spacing varying between 1 m and 5 m, with a typical value of 2 m.

The use of constant discharges to assess the consequences of flooding is justified by the morphology of the rivers studied. Indeed, as detailed by de Wit et al. (2007), the Meuse basin covers an area of about 33,000 km^2, including parts of France, Luxembourg, Belgium, Germany and the Netherlands. It can be subdivided into

three major geological zones, referred to as "Lotharingian Meuse" (southern part), "Ardennes Meuse" (central part) and the Dutch and Flemish lowlands (northern part).
While the southern and northern parts are characterized by wide floodplains where flood waves are significantly attenuated, in the central part of the Meuse basin, between Charleville-Mézières and Liège, the Meuse is captured in the Ardennes massif, characterized by narrow steep valleys, where flood waves are hardly attenuated.

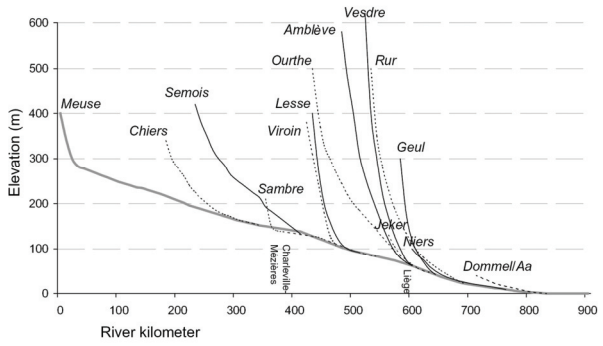

Fig. 3 River gradients of the Meuse and its tributaries. Adapted from de Wit et al. (2007) and Berger (1992).

The rivers considered hereafter are all situated in the central part of the Meuse basin. As shown in Fig. 3, the tributaries of river Meuse which flow in the Ardennes Massif present large river bed gradients. Consequently, the flood waves along this type of rivers are hardly attenuated as a result of the combination of the steep gradients and of the relatively narrow cross-sectional shape of the valleys (de Wit et al., 2007), leading to very low storage capacity in the floodplains. As a result the floodplains are completely filled with water quickly after the beginning of the flood and a quasi-steady flow is then observed.
For instance, for typical floods occurring on the river Ourthe, it has been verified that the volume of water stored in the inundated floodplains along a 10 km-long reach remains lower than one percent of the total amount of water brought by the flood wave.
Therefore, the steady-state assumption has been considered as valid for simulating floodplain inundation along most rivers of the Ardennes Massif. It has thus been systematically used in the simulations discussed in the subsequent paragraphs. An additional benefit of this assumption is a reduced run time as a result of the possibility to exploit automatic mesh refinement (§ 2.7).

5. RESULTS AND DISCUSSION

For the purpose of the hydraulic computation, the 800 km of rivers to be modelled have been divided into reaches 2 to 15-km long. The reaches have been delimited regarding hydraulic criteria for the prescription of the boundary conditions (weirs, bridges, etc) but also the consistency of the floodplain and the river bed topography features to facilitate the calibration of the roughness coefficients.
Fig. 4 illustrates the flood extension maps computed with a multiblock grid of 2 and 4 m on a 7.3-km long reach of the 69-km long river Dendre near Papignies, in the western part of Wallonia. The river Dendre is a tributary of the Scheldt and has a catchment area of 1,384 km². These results in terms of water depths, together with the distributed mean flow velocity fields also computed by the flow solver, fully characterise the inundation hazard. In the case of Fig. 4, despite the moderate variation in the flow rate, the maps show a substantial extension of the inundation along the river main bed. The details of the DEM allow determining accurately the location and the cause of overflowing as well as the local blockage effect of the railway embankment on the left for example. These results underline thus the precision in flood extension prediction reachable if the solver discretization features match the DEM characteristics.
Prior to the drawing of inundation maps, flood extension can be used for the validation of the computation method and the calibration of the roughness coefficient, such as along the river Lesse, located in the south-east of Belgium. This 89-km long river is a tributary of the river Meuse and has a catchment area of 1,343 km^2 and a mean annual discharge of 19 m^3/s at its mouth.
Fig. 5 and Fig. 6 compare the inundation extension along a meandering reach of the river for the flood of January 28th, 1995. The peak discharge has been evaluated at 180 m³/s, corresponding to a return period of 15 years. As shown by the reference points 1, 2 and 3 (Fig. 5 and Fig. 6), the predicted spatial pattern of inundation, simulated with a grid spacing of 2 m in the riverbed and 4 m in the floodplains, match observations very well. As a result of the field survey, the caravans in the campsite have been removed from the DEM as the water can flow under them (Point 2 – Fig. 6).

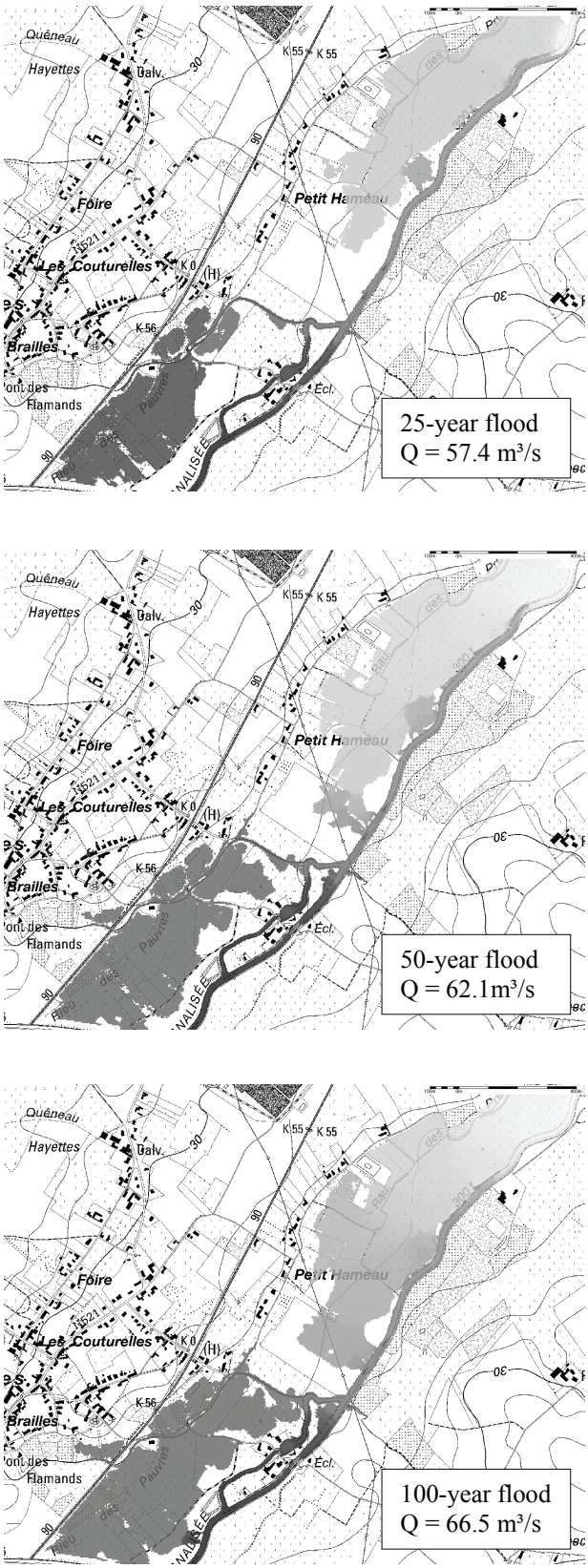

Fig. 4 Flood extension (topographical maps and water depths) on the river Dendre near Papignies for three statistical extreme floods.

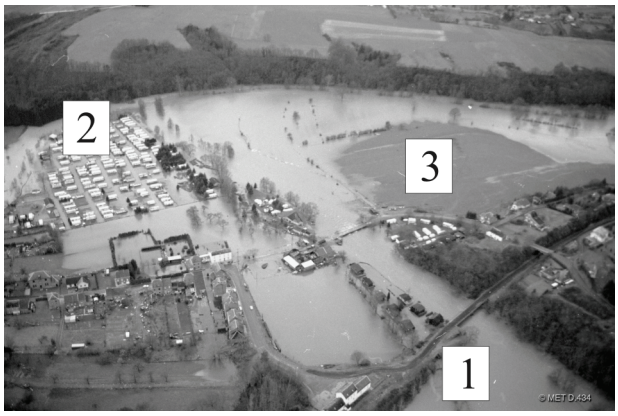

Fig. 5 Aerial photography of the inundation pattern along a meandering reach of the river Lesse on January 28th, 1995 - Discharge of 180 m³/s.

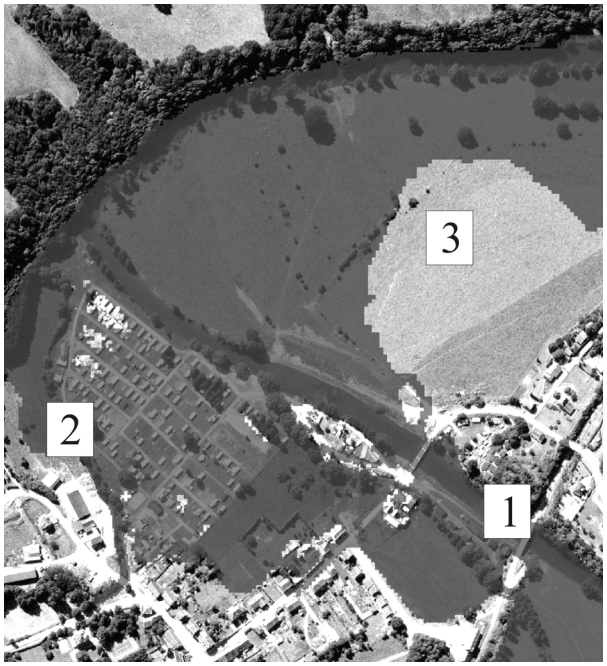

Fig. 6 Simulated inundation extent along a meandering reach of the river Lesse for the flood of January 28th, 1995 – Discharge of 180 m³/s.

Where comparison data are available, more quantitative validation can be performed, such as in the town of Han-sur-Lesse, along a 4-km long reach of the river. To take advantage of the finest DEM information in the town and around specific buildings such as existing flood protection walls, while limiting the number of computation cells, a multiblock grid has been used with meshes from 4 m down to 1 m (Fig. 7). The final computation grid counts for 450,000 finite volumes and covers an area of 1.256 km².

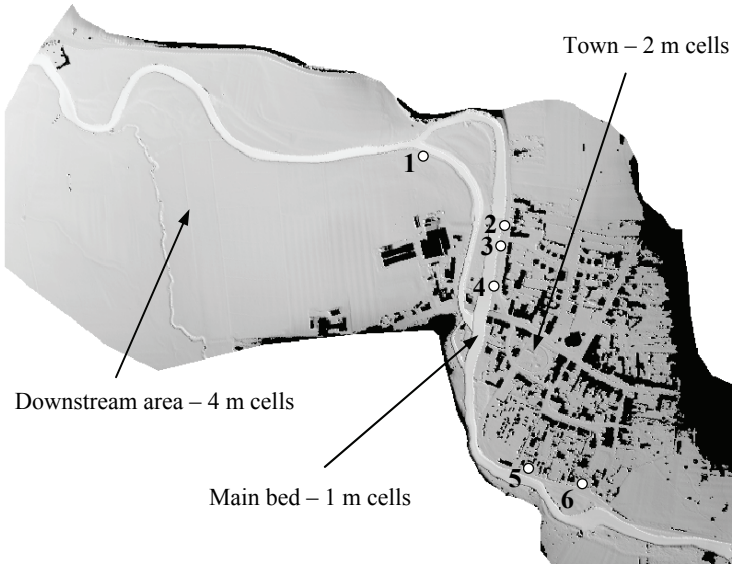

Fig. 7 DEM and computation cells size of the Lesse river near Han-sur-Lesse – Survey points for the flood of January 3rd, 2003.

Table 1 River Lesse near Han-sur-Lesse - Observed and computed water depths for the flood of January 3rd, 2003 – Discharge of 150 m³/s.

Survey point	Water depths [cm]	
	Observation	Calculation
1	82	86
2	5	15-30 at the centre of the street
3	25	5 along the houses
4	20	30
5	80	60
6	94	95

Fig. 8 Local acceleration of the flow on the river Lesse during the flood of January 3rd, 2003 – Discharge of 150 m³/s.

The flood of January 3rd, 2003 with a discharge of 150 m³/s is a real event usable for validation. Indeed, a field survey carried out after the flood provided relevant water levels data at 6 points to validate the numerical results (Fig. 7). The computed values match well the measured ones, even in the streets and near the houses, with a difference in the range of the DEM accuracy (Table 1).

In addition, the computation provides information on the flow regime which can be compared to pictures of the real event. For example, the flow acceleration upstream of a mill channel (Fig. 8) appears clearly in the numerical results (Fig. 9). This kind of results is of prime interest for policy makers to identify the priority area where interventions are needed to reduce flood risk.

Another example of such a quantitative comparison is on the river Amblève. This river springs in the eastern part of Belgium, close to the border with Germany, and flows towards the west

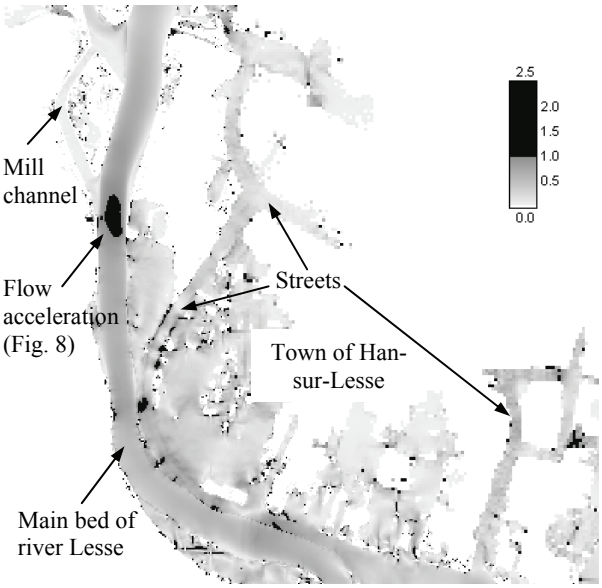

Fig. 9 Froude number distribution on the Lesse river near Han-sur-Lesse for the flood of January 3rd, 2003 – Discharge of 150 m³/s.

into the river Ourthe. It is 80-km long, has a mean annual discharge of 19.5 m^3/s at its mouth and a catchment area of 1,077 km^2.

During a flood in December 1993 (discharge: 298 m^3/s, return period: 10–15 years), water surface elevations have been measured at 11 locations along the most downstream reach of the river.

The comparison between this set of data and the predictions of the numerical model, with a grid spacing of 2 m everywhere, shows a satisfactory agreement, with an absolute error not exceeding 11 cm along the 12-km long considered reach (Fig. 10). Despite a single calibrated value of the roughness coefficient has been use for the whole length of the channel, the achieved accuracy is similar to the accuracy of the DEM (15 cm).

More detailed comparisons are presented in Fig. 11 and Table 2, focusing on a 3-km long reach nested in the above-mentioned one. They confirm that the simulated water depths match very well the measurements from the real event.

The repetitive computations of flow characteristics on the same river reaches for several discharges enable another interesting comparison of the numerical values with available real data.

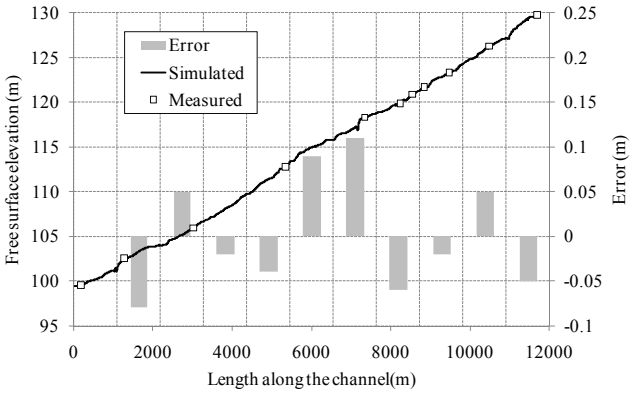

Fig. 10 Measured vs. simulated free surface elevations along a reach of the river Amblève during the flood of December 21st, 1993 – Discharge of 298 m^3/s.

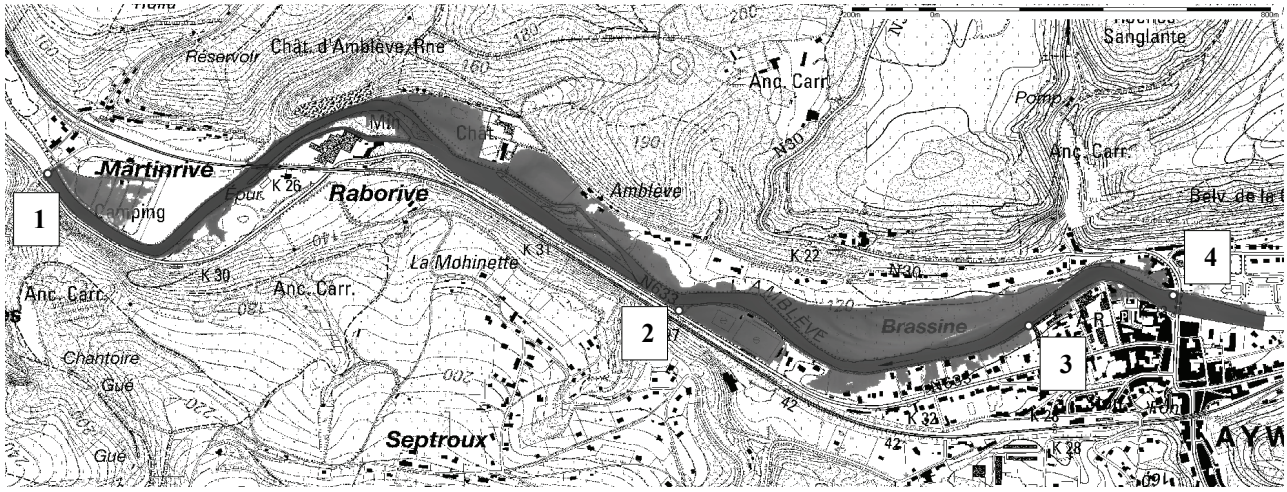

Fig. 11 Computed inundation extension during flood of the December 21st, 1993 on the river Amblève near Aywaille – Discharge of 298 m^3/s – Location of the 4 survey points.

Table 2 River Amblève near Aywaille – Observed and computed free surface elevations and corresponding water depths during the flood of Decembre 21st, 1993 – Discharge of 298 m^3/s.

	Location	Free surface elevation [m]		Water depths [cm]
		Observation	Calculation	Calculation
1	Downstream bridge	112.77	112.77	70
2	Football ground	118.38	118.40	110
3	School	119.81	119.85	20
4	Upstream bridge	120.81	120.85	60

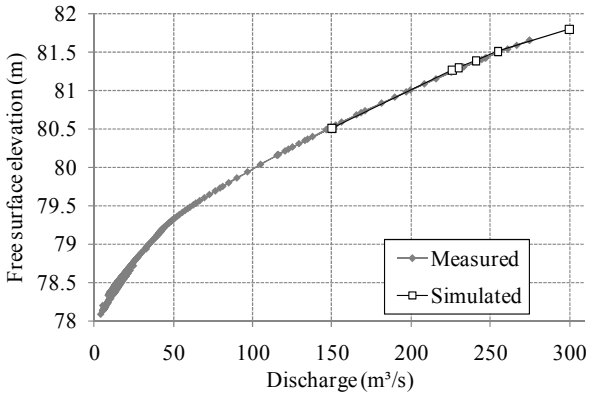

Fig. 12 Measured vs. simulated free surface elevations for different discharges on the river Vesdre.

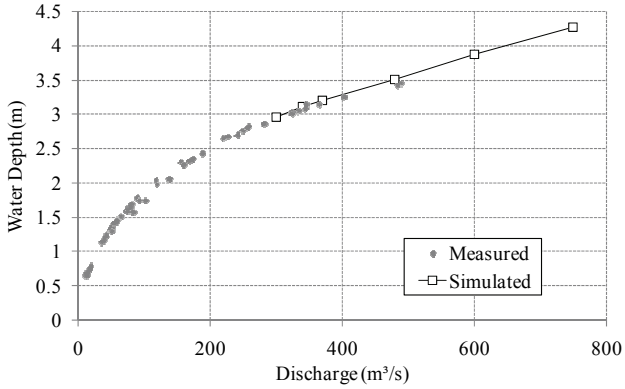

Fig. 13 Measured vs. simulated free surface elevation for different discharges on the river Semois.

The direct measurement of the discharge in a natural river is never possible. It is commonly performed by integration of a measured velocity profile on the flow section or by a water depth measurement and the use of a rating curve previously determined in a specific cross section. Usually, the first method is used during low flow periods and supplies the data necessary to compute the rating curve of the second method. By extrapolation, this last one is then used during high flows period where velocity profiles measurement is not convenient and sometimes even dangerous.

For the purpose of validation and calibration, the results of the numerical computations can be compared with existing rating curves. For example, Fig. 12 displays the measured stage-discharge relationship together with six points gained from numerical simulation on a 1-km long reach of the river Vesdre. This river is a 70-km long tributary of the river Ourthe and has a mean annual discharge of 12 m^3/s at its mouth for a catchment area of 700 km^2. The numerical model succeeds in predicting the water depth at the gauging station for a wide range of discharges (150–300 m^3/s). The simulations for the six discharge values have been performed with the same roughness coefficient, showing that no recalibration is necessary for such high discharges and as far as water depths in the main channel are considered.

A similar comparison has been performed for the river Semois, which is a 210-km long tributary of the river Meuse. Its catchment area is 1,350 km^2 and the mean annual discharge 35 m^3/s at its mouth. Again, the simulated water depths can be successfully compared with measurements for discharge values ranging between 300 m^3/s and 500 m^3/s (Fig. 13), without recalibration of the roughness coefficient. The hydraulic model has next been applied to extend the stage-discharge curve towards more extreme values in the range 500–800 m^3/s (Fig. 13). This provides an objective extrapolation of the rating curve to high water levels for which velocity profiles measurements are not possible.

6. CONCLUSIONS

An advanced 2D hydraulic numerical model has been presented. It is based on the fully dynamic shallow-water equations, solved by means of a finite volume scheme on multiblock structured grids. The simplicity and the efficiency of the numerical scheme make the model able to consider computation grids consisting of as many as one million meshes (3 millions unknowns) for steady state flow computations on natural topography. The only calibration parameter is the roughness coefficient, which can be spatially distributed both in the main riverbed and in the floodplains.

The model handles routinely highly accurate DEM derived from airborne laser altimetry for the floodplains and sonar detection for the bathymetry of the main channel. For river reaches as long as 10 to 15 km, the flow simulation may be performed with a grid spacing of 1 m, comparable to the resolution of the DEM and fine enough to represent reliably the flows at the scale of each building individually.

Consequently, the model succeeds in predicting accurately the local pattern of flood depths on a large part of the rivers in the south part of Belgium (800 km), as confirmed by several validation examples detailed in the paper. The applications demonstrate the ability of the model to predict the inundation extent and to reproduce

depth measurements for a wide range of flood discharges without the need for recalibration.

ACKNOWLEDGEMENTS

The authors gratefully acknowledge the Walloon Ministry of Facilities and Transport (MET) who provided the DEMs information and the pictures of real flood events.

NOTATIONS

$\mathbf{f}$	x-component of advective terms vector
$\mathbf{f}_d$	x-component of diffusive terms vector
g	gravity acceleration
$\mathbf{g}$	y-component of advective terms vector
$\mathbf{g}_d$	y-component of diffusive terms vector
h	water height
i	reference cell index
$i+1$	cell downstream of i cell index
n_b	Manning coefficient of the river bottom
n_w	Manning coefficient of the side walls
N_x	number of cell sides aligned along x-axis
N_y	number of cell sides aligned along y-axis
$\mathbf{s}$	unknowns vector
$\mathbf{S}_0$	bottom slope terms vector
$\mathbf{S}_f$	friction terms vector
t	time
u	average fluid velocity along x-direction
v	average fluid velocity along y-direction
x	x Cartesian coordinate
y	y Cartesian coordinate
Z	free surface elevation
z_b	bottom elevation
$\Delta\Sigma$	factor of increased friction area
Δx	mesh size along x-axis
Δy	mesh size along y-axis
ρ	water density
σ_x	turbulent normal stresses in x-direction
σ_y	turbulent normal stresses in y-direction
τ_{bx}	bottom shear stress along x-direction
τ_{by}	bottom shear stress along y-direction
τ_{xy}	turbulent shear stress

REFERENCES

1. Archambeau P (2006). *Contribution à la modélisation de la genèse et de la propagation des crues et inondations*. Ph.D. Thesis, HACH, University of Liège, Belgium. In French.
2. Audusse E (2004). *Modélisation hyperbolique et analyse numérique pour les écoulements en eaux peu profondes*. Ph.D. Thesis, Laboratoire Jacques-Louis Lions, Université Paris VI – Pierre et Marie Curie, France. In French.
3. Bates PD, De Roo APJ (2000). A simple raster-based model for flood inundation simulation. *Journal of Hydrology* 236:54–77.
4. Berger HEJ (1992). *Flow forecasting for the river Meuse*. Ph.D. Thesis, Delft University of Technology, The Netherlands.
5. Bradbrook K, Waller S, Morris D (2005). National floodplain mapping: datasets and methods – 160,000 km in 12 months. *Natural Hazards* 36:103–123.
6. Dewals BJ (2006). *Une approche unifiée pour la modélisation des écoulements à surface libre, de leur effet érosif sur une structure et de leur interaction avec divers constituants*. Ph.D. Thesis, HACH, University of Liège, Belgium. In French.
7. Dewals BJ, Erpicum S, Archambeau P, Detrembleur S, Pirotton M (2006). Depth-integrated flow modelling taking into account bottom curvature. *Journal of Hydraulic Research* 44(6):787–795.
8. Dewals BJ, Kantoush S, Erpicum S, Pirotton M, Schleiss A (2008a). Experimental and numerical analysis of flow instabilities in rectangular shallow basins. *Environmental Fluid Mechanics* 8:31–54.
9. Dewals BJ, Detrembleur S, Archambeau P, Erpicum S, Pirotton M (2008b). Detailed 2D hydrodynamic simulations as an onset for evaluating socio-economic impacts of floods considering climate change. In: Samuels, P., Huntington, S., Allsop, W., Harrop, J. (Eds.), *Flood Risk Management: Research and Practise*. Balkema, London, UK, pp. 125–135.
10. de Wit M, Peeters H, Gastaud P, Dewil P, Maeghe K, Baumgart J (2007). Floods in the Meuse basin: event description and an international view on ongoing measures. *International Journal of River Basin Management* 5(4):279–292.
11. Dutta D, Herath S, Musiake K (2003). A mathematical model for flood loss estimation. *Journal of Hydrology* 277(1–2):24–49.
12. Erpicum S (2006). *Optimisation objective de paramètres en écoulements turbulents à surface libre sur maillage multibloc*. Ph.D. Thesis, HACH, University of Liège, Belgium. In French.
13. Erpicum S, Archambeau P, Detrembleur S, Dewals BJ, Pirotton M (2007). A 2D finite volume multiblock flow solver applied to flood extension forecasting. In: Garcia-Navarro P, Playan E (Eds), *Numerical*

Modelling of Hydrodynamics for Water Resources. Taylor & Francis, London, pp. 321–325.
14. Fischer H, List E, Koh R, Imberger J, Brooks N (1979). *Mixing in Inland and Coastal Waters*. Academic Press, New York.
15. Hervouet J-M (2003). *Hydrodynamique des écoulements à surface libre – Modélisation numérique avec la méthode des éléments finis*. Presses de l'Ecole Nationale des Ponts et Chaussées, Paris. In French.
16. Lambert JD (1973). *Computational Methods in Ordinary Differential Equations*. John Wiley and Sons.
17. McMillan HK, Brasington J (2007). Reduced complexity strategies for modelling urban floodplain inundation. *Geomorphology* 90:226–243.
18. Merz R, Blöschl G, Humer G (2008). National flood discharge mapping in Austria. *Natural Hazards* 46:53–72.
19. Mignot E, Paquier A, Haider S (2006). Modelling floods in a dense urban area using 2D shallow water equations. *Journal of Hydrology* 327:186–199.
20. Nujic M (1995). Efficient implementation of non-oscillatory schemes for the computation of free-surface flows. *Journal of Hydraulic Research* 33(1):101–111.
21. Priestnall G, Jaafar J, Duncan A (2000). Extracting urban features from LIDAR digital surface models. *Computers, Environment and Urban Systems* 24:65–78.
22. Rastogi A, Rodi W (1978). Predictions of heat and mass transfer in open channels. *Journal of the Hydraulics Division, ASCE* 104(HY3):397–420.
23. Rodi W (1984). *Turbulence Models and Their Application in Hydraulics – A State-of-the-Art Review* (second revised edition). Balkema, Leiden.
24. Sanders B (2007). Evaluation of on-line DEMs for flood inundation modeling. *Advances in Water Resources* 30:1831–1843.
25. Soares Frazão S (2000). *Dam-break induced flows in complex topographies – Theoretical, numerical and experimental approaches*. Ph.D. Thesis, Université Catholique de Louvain, Belgium.